Int. J. Heat Mass Transfer. Vol. 36, No. 5, pp. 1367–1372, 1993
Printed in Great Britain

0017–9310/93 $6.00 + 0.00

Two-phase flow in the localized boiling field adjacent to a heated wall

F. BONETTO, A. CLAUSSE and J. CONVERTI
Centro Atomico Bariloche, 8400-Bariloche, Argentina

(*Received* 4 *June* 1991 *and in final form* 19 *May* 1992)

Abstract—An experiment performed in a small horizontal heater immersed in refrigerant FC-72 is presented. The spatial distribution of the vapor is measured using a hot wire anemometer located over the heater, for different heat power inputs. The experimental data are analyzed using a probabilistic model to obtain information about the void fraction, bubble size and vapor velocity. A theoretical model based in conservation equations is derived which accounts for a comprehensive description of the experimental results. Moreover, a unified explanation of the interrelation between the mechanisms of nucleate boiling and boiling crisis is concluded.

INTRODUCTION

THE PROBLEM of boiling is one of the most complicated in heat transfer theory. As Lienhard [1] has recently mentioned, we still cannot predict from first principles the heat flux-wall temperature relation for a given geometry. The numerous reported studies of boiling at low and high heat fluxes have generally been given in the form of correlations. It has been possible to identify the similarity groups associated with the CHF process [2]. However, at present no closed analytical solution exists for the intensive turbulent heat transfer with vapor bubble generation and their departure from the heating surface.

The well-known Rohsenow [3] correlation has been rather successful in predicting the observed nucleate boiling data. This correlation is based on a simple mechanistic model, though its success is due to the right combination of the correct length scale with appropriate thermophysical properties. Subsequently, different mechanisms were proposed by other authors [4] with some success, but none of great significance. The main reason for the limited success of those attempts is the lack of understanding of the interaction between surface and fluid parameters.

On the other hand, the problem of the critical heat flux was always treated as a phenomenon independent from the nucleate boiling process, and almost nothing is known about their interrelation. A number of theoretical predictions of the critical heat flux in pool boiling, based on hydrodynamic instability considerations, were proposed in the past [2, 5]. All these theoretical equations are similar to one another and they agree equally well with the experimental data.

For the nucleate boiling heat transfer, it has generally been accepted that the dynamics of the liquid and gas components close to the wall is of primary importance. Therefore, it is not surprising that most of the proposed theoretical models involve in the calculations hydrodynamic quantities as void fraction, bubble density, frequency, site density, gas velocity. However, only comparisons with the heat flux wall superheating relation and physical properties is performed to validate the theory. One reason for this is the lack of experimental data related to the hydrodynamics parameters.

In boiling two-phase flow, it is of considerable importance to know the phase distribution near the wall. For example, the presence of vapor affects the neutron moderation and therefore the fission rate in nuclear power plants. Lian and Dhir [6] measured the void fraction averaged in a line as a function of the distance from a vertical heater plate with an X-ray attenuation technique. They found that for high heat fluxes, the void fraction as a function of the distance from the heater presents a maximum near the wall.

The purpose of the present work is to contribute to the development of mechanistic models of nucleate boiling and boiling crisis by studying experimentally the interplay between the heat flux and the vapor flow dynamics close to a heated surface. An experiment performed in a small horizontal heater immersed in dielectric refrigerant FC-72 is described. The spatial distribution of the vapor during the boiling process is measured using a hot wire anemometer located over the heater. Series of data were taken with the anemometer at different heat fluxes. The data are analyzed and compared with a theoretical model for void fraction, interfacial area and vapor velocity close to the wall.

EXPERIMENTAL APPARATUS AND PROCEDURE

The experimental apparatus used in this investigation is shown schematically in Fig. 1. A tank 273 mm × 127 mm base and 152 mm high containing the test section, the working fluid, and a cartridge heater for degassing was placed in a water jacket, which could be heated up to the desired temperature through its connections to a refrigerated/heating circulating

NOMENCLATURE

A	heated area
a_i	interfacial area density
b	characteristic rate of breakup
$\mathscr{B}$	breakup rate
c	characteristic rate of coalescence
C_D	drag coefficient
CV	control volume
$\mathscr{C}$	coalescence rate
g	gravity
h_{fg}	latent heat of evaporation
k	coefficient defined in equation (15)
n	number of bubbles per unit volume
q''	heat flux
$\hat{q}''$	dimensionless heat flux $(36\pi/\mathscr{V}_c)^{1/6}(C_D/8g)^{1/2}(q''/\rho_g h_{fg})$
q''_{CHF}	critical heat flux
q_{nv}	heat which does not produce vapor inside the CV
t_{ng}	period during which the probe is in liquid
T	measurement time
T_g	period during which the probe is in gas
T_{ng}	probability of no gas interception
r_b	bubble radius
u	gas velocity
$\mathscr{V}_b$	bubble volume
$\mathscr{V}_c$	critical volume of breakup
$\mathscr{V}_o$	characteristic volume parameter, k/Ah_{fg}
z	spatial variable.

Greek symbols

α	void fraction
α_{CHF}	void fraction at the critical heat flux
Γ	evaporation rate
ρ_g	vapor density
ρ_l	liquid density
τ	signal time.

Superscript

$\hat{}$	dimensionless.

bath. All the experiments were carried out at saturation temperature, 56°C. The vapor generated at the test section was condensed back to the pool by a vapor space coil and a reflux condenser cooled by tap water. The test section was positioned in the tank so as to ensure no side wall blockage or immersion depth effects.

The direct current power supplied to the test section was evaluated by measuring the current and the voltage drop across the heater. Two thermocouples were used to monitor the pool temperature, one in a fixed position about 3 cm below the boiling surface and the other movable to check for temperature gradients.

A circuit board (glass epoxy G-10) with copper cladding on one side was used as the substrate. The copper cladding in the center was removed by etching to make room for the 25.4 μm-thick nichrome foil heater. The foil was then soldered to the copper cladding for the electrical connections. A 4 cm Plexiglas block was bonded to the back side of the circuit board for insulation. A smooth copper block 5 × 5 × 1.5 mm was attached to the former using M-Bond 610 epoxy. After soldering the foil to the copper cladding, a layer of epoxy was used to guard the sides of the copper block.

A hot wire anemometer TSI 25 μm was allowed to move above the heated section. The hot wire was at the heater center on the horizontal plane. A traversing mechanism was used to position the hot wire in the vertical direction (Fig. 1). The hot wire gives a different signal whether liquid or gas is present at the tip. The output signal was digitized and recorded using an IBM-PC computer with a 5 kHz sampling frequency. The resulting signal is a logical 1 when gas is present at the probe tip and a logical 0 when liquid is present at the probe tip (this is often called the *indicator function*).

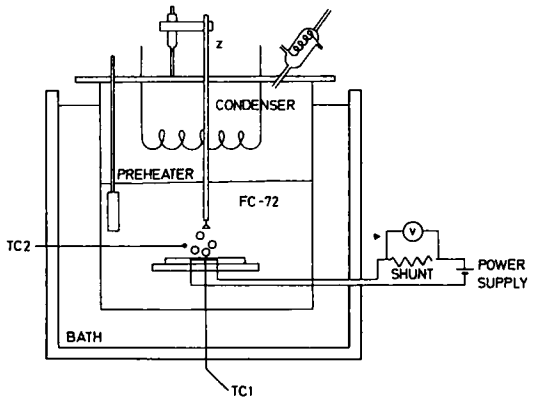

FIG. 1. Diagram of the experimental apparatus.

ANALYSIS OF THE EXPERIMENTAL RESULTS

The indicator function signal was recorded for different heat fluxes. The probe was located at different positions to map the spatial distribution effects. A probabilistic model was developed to analyze the information contained in the signal provided by the probe. The objective of the analysis is to relate the signal with the local two-phase flow parameters in the point where the probe is placed.

VOID FRACTION

The first physical parameter which can be obtained from the experimental signal is the local void fraction,

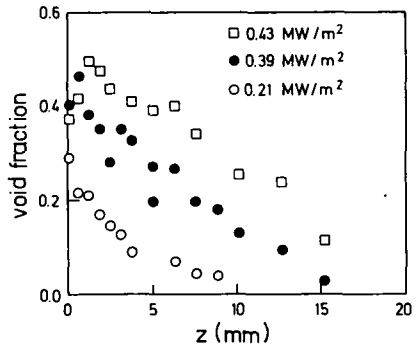

FIG. 2. Void fraction dependence with the distance from the heater.

α. Integrating the probe signal in time, we can calculate the void fraction by

$$\alpha = \frac{T_g}{T} \tag{1}$$

where T_g is the period of time during which the probe is in gas, and T is the total time of measurement. From the point of view of a statistical description, the local void fraction can be interpreted as the probability of finding gas in a certain position.

The dependence of α with the distance from the wall z is depicted in Fig. 2 for different heat fluxes. For low heat fluxes the void fraction decreases monotonically. However, as the critical heat flux is approached, a void fraction peak appears near the wall.

Figure 3 shows the void fraction as a function of the heat flux. This curve corresponds to a position located at the center of the heater and $z = 2$ mm. As can be easily seen, the void fraction increases with the heat flux.

PROBABILITY DENSITY FUNCTION OF NO GAS INTERCEPTION

Besides the void fraction it is desirable to obtain more information about the boiling two-phase flow field from the signal statistics. For the purpose of a first approach to the problem, let us consider the probe as a fixed point in a field of identical spherical bubbles rising with the same velocity, u. The problem can be thought of as if the probe is moving down with velocity u in a liquid field covered by a dispersion of gas spheres with a uniform probability distribution. Figure 4 illustrates this situation. It can be seen that only the bubbles whose centers are contained in the cylinder of radius r and axis coincident with the probe path are detected.

If the probe intercepts the horizontal diameter of a sphere in $z = 0$, the probability $P(z)$ of not intercepting any horizontal diameter along a probe path length z satisfies:

$$P(z+\mathrm{d}z) = (1-\mathrm{d}p_i)P(z) \tag{2}$$

where $\mathrm{d}p_i$ is the probability of finding a center in an infinitesimal slice of a cylinder of radius r (see Fig. 4), given by:

$$\mathrm{d}p_i = n\pi r^2\,\mathrm{d}z. \tag{3}$$

Combining equations (2) and (3) yields

$$\frac{\mathrm{d}P}{\mathrm{d}z} = -n\pi r^2 P. \tag{4}$$

Integrating equation(4) gives

$$P(z) = \mathrm{e}^{-n\pi r^2 z} \tag{5}$$

where $P(0) = 1$ was used.

The distance z traveled by the probe corresponds to the time interval τ of the signal according to

$$z = u\tau. \tag{6}$$

Combining equations (5) and (6), the probability that during the time τ no bubble horizontal diameter touches the probe is given by

$$P(\tau) = \mathrm{e}^{-n\pi r^2 u\tau}. \tag{7}$$

The mean value of the intervals between bubble centers is given by

$$\langle\tau\rangle = \int_0^\infty P(\tau)\tau\,\mathrm{d}\tau = (\pi n r^2 u)^{-1}. \tag{8}$$

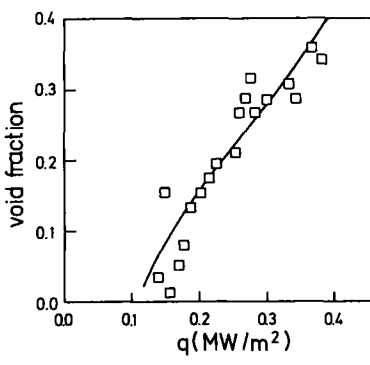

FIG. 3. Void fraction as a function of heat flux ($z = 2$ mm).

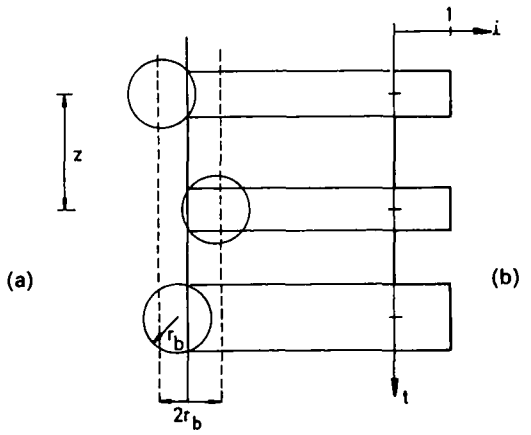

FIG. 4. Relation between the bubble distribution (a) and the probe signal (b).

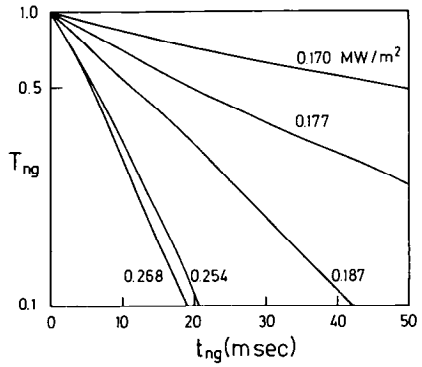

FIG. 5. Probability of no gas interception (T_{ng}) during a measuring time t_{ng} ($z = 2$ mm).

Let us now define the probability density function, T_{ng} of not having bubbles intercepting the probe during a time interval t_{ng} (ng stands for 'no gas'). This is a problem similar to radioactive decay and T_{ng} is similar to the probability of no decay during a certain time interval. Therefore by analogy T_{ng} is given by

$$T_{ng} = \exp(-t_{ng}/\langle\tau\rangle). \tag{9}$$

The distribution T_{ng} is calculated from the experimental signal as follows. The center of each bubble interception was marked in the time axis. A window of width t_{ng} was chosen and it was moved along the time axis. In each position, the existence of any mark was checked. The absence of a mark was considered a favorable event. The number of favorable events divided by all the tries gives the probability of no bubble center at the probe during the time t_{ng}.

Figure 5 displays T_{ng} for different heat fluxes. As q'' increases the average time between successive bubbles decreases. Equations (8) and (9) relate the slope of the T_{ng} distribution in logarithmic scale with the local two-phase flow parameters (r, n, u). Figure 6 shows $\langle\tau\rangle$ as a function of q''.

The analysis predicts that the probability of no bubble's center interception during a time interval t_{ng} follows an exponential law. The exponential law has a strong dependence with the hypothesis that bubble centers have a uniform random distribution. The χ^2 test was used to check the agreement of the data with an exponential distribution. The exponential law turned out to be true with a 5% significance level, therefore supporting the hypothesis of random distribution of bubbles.

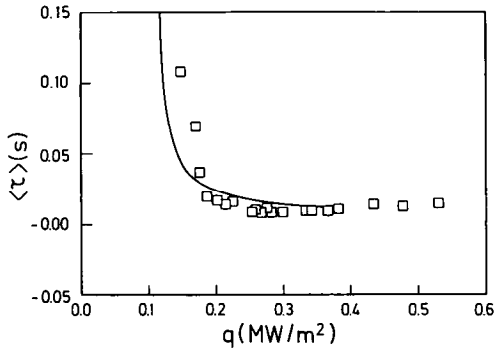

FIG. 6. Mean value of the intervals between bubble centers, $\langle\tau\rangle$, as a function of the heat flux ($z = 2$ mm).

A PHYSICAL INTERPRETATION OF THE RESULTS

To understand the experimental results based on basic conservation equations, a theoretical analysis of the local boiling process was performed. Let us consider the simplest approximation consisting of a horizontal plate heater providing a heat flux q'' to a pool of liquid at saturated temperature (Fig. 7). A control volume (CV) is defined on top of the surface. The two-phase flow variables are averaged in the CV [7]. Assuming that the CV contains n identical spherical bubbles per unit volume, the void fraction, α, the specific interfacial area density, a_i, and the bubble volume, $\forall_b$, are given by:

$$\alpha = n\forall_b \tag{10a}$$

$$a_i = n4\pi r_b^2 \tag{10b}$$

$$\forall_b = \tfrac{4}{3}\pi r_b^3 \tag{10c}$$

where r_b is the bubble radius.

The objective of the analysis is to find a relation between the average two-phase flow parameters in the local CV and the heat flux, q''. The starting points are the momentum, mass, and energy balances over the CV.

Vapor momentum balance

Once the rising bubble velocity is reached, the buoyancy force on the bubble is balanced by drag force acting on the liquid–gas interface, that is

$$g(\rho_l - \rho_g)\forall_b = C_D(\pi r_b^2)[\tfrac{1}{2}\rho_l u^2] \tag{11}$$

where C_D is the drag coefficient.

Assuming that the gas density, ρ_g, is negligible compared to the liquid density, ρ_l, yields

$$2g\forall_b = \pi C_D u^2 r_b^2. \tag{12}$$

Combining equations (10) and (12) gives

$$8g\alpha = C_D a_i u^2. \tag{13}$$

Vapor mass balance

At steady state, the vapor mass entering the CV is equal to the vapor mass leaving the CV, that is

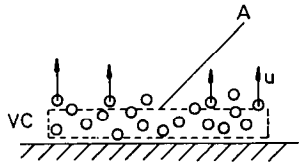

FIG. 7. Diagram of the theoretical model.

$$\Gamma = \alpha A u \rho_q \tag{14}$$

where Γ is the evaporation rate inside the CV.

Energy balance

The total heat power input is partitioned in heat that produces vapor inside the CV and the rest which is transported by microconvection, Marangoni effect, or any other mechanism different from evaporation inside the CV. The latter is assumed to be promoted by the vapor mass flow $\rho_g u \alpha A$, leaving the CV and to increase as the number of bubbles in the CV increases. A simple model describing this trend is

$$q_{nv} = k \rho_g u \alpha n \tag{15}$$

where k is a constant coefficient.

The total heat power is partitioned as

$$q'' A = \Gamma h_{fg} + k \rho_g \alpha u n. \tag{16}$$

The first term of the right-hand side corresponds to the heat power necessary to produce an evaporation rate Γ inside the CV.

Combining equations (14) and (16) yields

$$\frac{q''}{\rho_g h_{fg}} = (1 + \forall_o^{\cdot} n) u \alpha \tag{17}$$

where $\forall_o^{\cdot} = k/A h_{fg}$ is a characteristic volume parameter.

Combining equations (10), (13) and (17) gives

$$\alpha^7 = 36\pi (C_D/8g)^3 (q''/\rho_g h_{fg})^6 \frac{n}{(1 + \forall_o^{\cdot} n^6)}. \tag{18}$$

Interfacial area

A few empirical correlations for the interfacial area density, a_i, are available for relatively small void fractions [8]. However, the idea of a conservation equation for a_i based on a mechanistic model that includes the dynamics of the breakup and coalescence processes for the dispersed bubbles, has been recently suggested [9]. For consideration of the processes of bubble coalescence and breakup it is convenient to write a conservation equation for the number of bubbles per unit of volume, n. Because of the lack of sufficient information, the rate of breakup per unit of volume, $\mathscr{B}$, and the rate of coalescence, $\mathscr{C}$, are modeled here based on general experimental trends.

Coalescence. The coalescence rate is proportional to n^2 and to the probability of collision. The probability of collision of two bubbles may be taken to be proportional to the bubble volume, $\forall_b^{\cdot}$ [10]. The physical meaning of this assumption is that having two bubbles in a box, the probability of coalescence is proportional to the volume they occupy. Thus the total coalescence rate in the control volume is given by

$$\mathscr{C} = c \forall_b^{\cdot} n^2 \tag{19}$$

where c is a characteristic constant rate.

Breakup. The shattering probability of a bubble is modeled in such a way that is very low for a bubble having a volume $\forall_b^{\cdot}$ smaller than a critical volume $\forall_c^{\cdot}$, while for larger bubbles breakup is most likely to occur. Following this trend, we propose

$$\mathscr{B} = bn \frac{\forall_b^{\cdot 2}}{\forall_b^{\cdot 2} + \forall_c^{\cdot 2}} \tag{20}$$

where b is a characteristic constant rate.

At steady state the rate of breakup is balanced by the rate of coalescence, that is

$$c \forall_b^{\cdot} n^2 = bn \frac{\forall_b^{\cdot 2}}{\forall_b^{\cdot 2} + \forall_c^{\cdot 2}}. \tag{21}$$

Combining equations (10) and (21) gives

$$\forall_c^{\cdot 2} n^2 = \alpha (b/c - \alpha). \tag{22}$$

COMPARISON WITH THE EXPERIMENTS

Equations (18) and (22) can be used to calculate the values of α and n for a given q''. Defining the dimensionless bubble number density

$$\hat{n} = n \forall_c^{\cdot} \tag{23}$$

equations (18) and (22) become

$$\alpha^7 = \hat{q}''^6 \frac{\hat{n}}{(1 + \hat{n} \forall_o^{\cdot} / \forall_c^{\cdot})^6} \tag{24a}$$

$$\hat{n}^2 = \alpha (b/c - \alpha). \tag{24b}$$

Figure 8 shows the behavior of equations (24) in the (α, n) plane, for boiling in refrigerant FC-72. Equation (24b) describes a semicircle in the ($\hat{n}$, α) plane. The physical meaning of this trend can be understood as a competition between the mechanisms of bubble coalescence and breakup. For low void fractions the breakup process prevails, increasing the number of bubbles as the void fraction (i.e. the amount of vapor) increases. At higher void fractions the rate of coalescence becomes important inducing a process of vapor clustering in large bubbles, which reduces the number of bubbles as the void fraction increases. The dashed curves correspond to equation (24a) for different heat fluxes. The intersections of the curves give the void fraction, α, and the number density, $\hat{n}$, in the CV when a certain heat flux is imposed. At low heat fluxes [curve (a)] only one solution exists, and it can be verified that the void fraction in the CV increases with q''. However, n presents a maximum as the heat flux increases, which is a consequence of the competition of the mechanisms of bubble breakup and coalescence.

An interesting feature occurs for higher heat fluxes [curve (c)], for which three possible steady state solutions coexist for a given q''. The solution with the highest α corresponds to a very small n, which implies a large bubble volume, $\forall_b^{\cdot}$ [see equation (10a)]. This in turn can be seen as the coalescence of all the vapor in a film near the heater surface. Therefore, this state

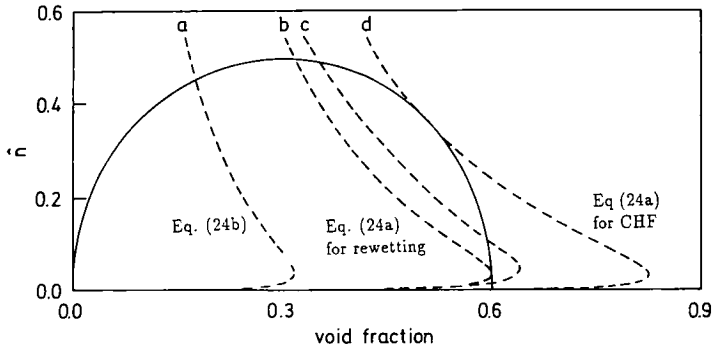

FIG. 8. Theoretical relation between the number of bubbles and the void fraction [equations (24)]. The dashed curves correspond to equation (24a) for heat fluxes increasing from (a) to (d).

can be interpreted as a film boiling regime. The intermediate solution corresponds to an unstable point (saddle point) which can be interpreted as a boiling transition regime. Following this interpretation, the curve (d) in Fig. 8 corresponds to the critical heat flux, since for higher q'' only the film boiling solution is possible.

The measured critical heat flux and the correspondent void fraction adjacent to the wall are

$$q''_{CHF} = 0.4\,\mathrm{MW\,m^{-2}}$$

$$\alpha_{CHF} = 0.42.$$

The point $(q''_{CHF}, \alpha_{CHF})$ can be used to fit the values of the remaining unknown parameters in equations (24). The resulting values are

$$b/c = 0.6$$

$$\mathscr{V}_o/\mathscr{V}_c = 8.75.$$

Using these values, the void fraction as a function of the heat flux can be calculated from equations (24). The resulting curve is compared with the experimental data in Fig. 3.

The theoretical model can also predict the experimental mean parameter $\langle\tau\rangle$ calculated with equation (8). Combining equations (8) and (10), yields

$$\langle\tau\rangle^3 = \frac{48^2}{\pi u^3 n \alpha^2}.$$

Calculating n, u and α from equations (17), (18) and (22), the value of $\langle\tau\rangle$ can be obtained for each q''. In Fig. 6 the theoretical result is compared with the experiment.

Another interesting feature of the theoretical model solutions can be found by decreasing the heat flux from curve (c) to curve (b). Curve (b) can be interpreted as the Leidenfrost point of rewetting, since for further decrease of q'', the film boiling solution no longer exists [see curve (a)]. The value of the Leidenfrost point heat flux predicted by the equations (24) is 0.24 MW m^{-2}, which is within the error band of the measured value $(q''_L)_{exp} = (0.26 \pm 0.03)$ MW m^{-2}.

CONCLUSIONS

Detailed experimental data of the two-phase flow field in the boiling region over a heated wall were presented. The experimental signal provided by a hot wire anemometer probe was statistically analyzed. Information about void fraction, bubble size and vapor velocity was obtained.

A theoretical model based on conservation equations was derived and compared with the experimental data. Good agreement was found within the expected uncertainties. Moreover, the model presents unified explanation of the interrelation between the mechanisms of nucleate boiling and boiling crisis. Further improvements of the theory may lead to a comprehensive mathematical description of the different aspects of the boiling process.

Acknowledgements—The authors wish to thank Ricardo Carvalho and Arthur E. Bergles from Rensselaer Polytechnic Institute for their kind collaboration in this research.

REFERENCES

1. J. Lienhard, Things we don't know about boiling heat transfer: 1988, *Int. Commun. Heat Mass Transfer* **15,** 401–428 (1988).
2. S. Kutateladze, On the transition to film boiling under natural convection, *Kotloturbostroenie* **3,** 10 (1948).
3. W. Rohsenow, *Trans. ASME* **74,** 969 (1952).
4. S. Van Stralen and R. Cole, *Boiling Phenomena.* McGraw-Hill, New York (1979).
5. N. Zuber, On the stability of boiling heat transfer, *Trans. ASME* **80,** 711 (1958).
6. S. P. Lian and V. K. Dhir, Void fraction measurements during saturated pool boiling of water on partially wetted vertical surfaces, *J. Heat Transfer* **111,** 731–738 (1989).
7. J. M. Delhaye, Equations fondamentales des Ecoulements diphasiques, Partes 1 et 2, CEA-R-3429, Centre d'Etudes Nucléaires de Grenoble, France (1968).
8. I. Kataoka and A. Serizawa, Interfacial area concentration in bubble flows, *Nucl. Engng Des.* **120,** 163 (1990).
9. S. Valenti, A. Clausse, D. Drew and R. T. Lahey, A contribution to the mathematical modeling of bubbly-slug flow regime transition, *Chem. Engng Commun.* **102,** 69–85 (1991).
10. G. Manucci, A theory of coalescence, *Chem. Engng Sci.* **24,** 975 (1969).